Journal of Hydrology 591 (2020) 125590

Contents lists available at ScienceDirect

Journal of Hydrology

journal homepage: www.elsevier.com/locate/jhydrol

Research papers

Carbon biogeochemical processes in a subtropical karst river–reservoir system

Wanfa Wang[a,1], Yuanbi Yi[a,1], Jun Zhong[a,*], Amit Kumar[b], Si-Liang Li[a,c]

[a] Institute of Surface-Earth System Science, School of Earth System Science, Tianjin University, Tianjin 300072, China
[b] School of Hydrology and Water Resources, Nanjing University of Information Science and Technology, Nanjing 210044, China
[c] State Key Laboratory of Hydraulic Engineering Simulation and Safety, Tianjin University, Tianjin 300072, China

ARTICLE INFO

Keywords:
Dissolved inorganic carbon
Carbon isotope
Reservoir effect index
Cascade reservoirs
Karst

ABSTRACT

Cascade damming has seriously affected the hydrologic regimes and solutes transport of the river systems. However, the effect of damming on carbon cycle and the underlying mechanisms are still unclear. In this study, to reveal the effects of damming on riverine dissolved inorganic carbon (DIC) transport, the water chemistry and stable isotopic signature of dissolved inorganic carbon ($\delta^{13}C_{DIC}$) were analyzed in the tributaries and four subtropical karst reservoirs on the Pearl River in southern China. From reservoir epilimnion to hypolimnion, DIC concentrations increased from 183.2 to 229.4 mg L^{-1}, 167.6 to 192.0 mg L^{-1}, 179.1 to 181.5 mg L^{-1}, and 182.4 to 183.8 mg L^{-1} while $\delta^{13}C_{DIC}$ decreased from −6.6‰ to −9.7‰, −7.8‰ to −10.4‰, −9.7‰ to −10.0‰ and −9.9‰ to −10.0‰ in the Chaishitan (CST), Longtan (LT), Yantan (YT), and Dahua (DH) reservoirs, respectively. Our analyses suggest that primary production and organic matter degradation were two dominant processes in carbon evolution in the epilimnion and hypolimnion, respectively. However, there was no obvious spatial heterogeneity of solutes' concentration in the DH reservoir. Our results also suggested that cascade reservoirs had a regional damming effect and could be significantly weakened without damming or in daily regulated reservoirs. Furthermore, $\delta^{13}C_{DIC}$ had a significant positive relationship with the reservoir effect index (*Ri*), which was affected by hydraulic retention time and water temperature in the water column of reservoirs and is useful to evaluate the thermal stratification strength. This study highlights that dam constructions affected carbon transport and transformation significantly, and the degree of the damming effect on the carbon cycle can be expressed by *Ri*.

1. Introduction

Reservoirs are used for flood control, irrigation, navigation, and electricity generation, and are considered as green sources of energy (Yoshikawa et al., 2014; Tockner and Stanford, 2002). Hydropower contributes about 16.6% of the world's electricity generation from renewable sources (REN21, 2016). Over the past several decades, the number of dams constructed has increased dramatically at regional and global levels, thereby rivers are under sustained pressure, such as the losses of river connectivity, a rapid decline of biodiversity, increases in sediment extraction, and emitting a significant amount of greenhouse gases to the atmosphere (Cardinale et al., 2012; Grill et al., 2019; Maavara et al., 2020; St. Louis et al., 2000). Therefore, the damming effect has attracted substantial attention from researchers worldwide to think about a sustainable environment in the future (Dams, 2000).

Rivers are the main channel for material, especially carbon, transportation from the land to the ocean (Cole et al., 2007). About 900 Tg yr^{-1} (1 Tg = 1 × 10^{12} g) of terrestrial carbon is transported to the ocean through rivers, of which inorganic carbon makes up about 450 Tg (Cole et al., 2007; John, 1992; Meybeck, 1982). However, due to artificial regulation, free-flowing large rivers in the world are not more than one third currently, which would contribute large shares to the regional or global carbon budgets (Grill et al., 2019; Maavara et al., 2017; Mendonça et al., 2017). St. Louis et al. (2000) reported that the average fluxes of CO_2 and CH_4 in tropical reservoirs are more than 4 times and 10 times higher than the global lake system, respectively. The reservoir surface water samples loss 20% of DIC in the reservoir surface water compared with the released water in the wet season of some karst stratified reservoirs in the Wujiang River (Wang et al., 2020). It is suggested that the damming effect seriously changed the geochemical

* Corresponding author.
E-mail address: jun.zhong@tju.edu.cn (J. Zhong).
[1] These authors contributed equally to this work.

https://doi.org/10.1016/j.jhydrol.2020.125590

Available online 01 October 2020

Table 1
The salient characteristics of studied reservoirs.

Reservoirs	Average air temperature (°C)	Average sampling depth (m)	Elevation (m)	Age of the reservoirs (yr)	Hydraulic retention time (day)	Average inflow ($m^3\ s^{-1}$)	Average annual discharge ($m^3\ s^{-1}$)	Capacity ($10^8 m^3$)	Catchment (km^2)	Stratified status	Drainage basin
CST	18.1	51	1640	20	103	31.5	48.4	4.37	4556	incomplete	mainstream
LT	22.1	126	400	11	193	1777.8	1639.4	273	98,500	incomplete	mainstream
YT	24.6	51	223	28	21	1464.6	1760.0	33.8	106,580	monthly	mainstream
DH	24.6	34	155	34	5	1796.8	1990.0	9.64	112,200	daily	mainstream

behavior of carbon, which formed a unique river–reservoir system and has gained great attention from researchers worldwide (Barros et al., 2011; Maavara et al., 2020). In recent years, many studies have been carried out on hydrology, organic matter burial, sediment interception, and GHGs in the river–reservoir systems (Barros et al., 2011; Best, 2018; Kondolf et al., 2014; Wang et al., 2018, 2019a). The literature has revealed that hydraulic retention time (HRT), water depth, and nutrient retention of rivers would be changed by damming, which may contribute to the increase of bicarbonate fluxes from river to ocean (Olden and Naiman, 2010; Wang et al., 2020). Although a few studies have been reported to evaluate the impact of reservoirs with specific indicators (Barros et al., 2011; St. Louis et al., 2000; Liang et al., 2019), the influence of cascade reservoirs on the carbon cycle is still unclear. It is an important way to integrate more studies into comparative analysis to explore the damming effect on the carbon cycle. However, a lack of good indicators would lead to the research on reservoirs being too scattered to be effectively integrated. While compared with a single reservoir, cascade reservoirs may have a regional damming effect, which is mainly reflected in the great difference of water chemistry in the different areas of the reservoir (Fan et al., 2015; Wang et al., 2020). Therefore, it is urgent to understand the potential effect of river damming on carbon transportation and conduct systematic studies on carbon biogeochemical processes in the river–reservoir system to understand the inherent processes and key factors affecting carbon distribution.

ICOLD (2018) reported that about 23,842 reservoirs with a dam height of ≥15 m existed in China, of which more than 68% of dams have been established in south China. Moreover, the largest karst area in the world is in southwestern China, which accounts for 15.6% of the world's total karst area (Ford and Williams, 2007; Jiang et al., 2014). Karst areas are more sensitive to climate change than non-karst areas, which are regarded as an important carbon sink area through the weathering of carbonate rocks (Beaulieu et al., 2012; Liu et al., 2016). Carbonate weathering can consume carbon dioxide (CO_2) from the atmosphere and release dissolved inorganic carbon (DIC) into the water bodies (e.g., rivers, reservoirs, lakes), which is an important part of the global carbon cycle (Gaillardet et al., 2019; Zhong et al., 2020). However, following the damming of the karst rivers, DIC was severely affected by primary production, carbonate precipitation, CO_2 outgassing and other biogeochemical processes (Liu et al., 2018; Wang et al., 2019b). In this study, four typical karst reservoirs have been studied which were on the Pearl River, the second largest river in China. This is the first comprehensive study on the cascade reservoirs in the upstream of the Pearl River where the air temperature is high all year round by the influence of the subtropical monsoon climate. Further, systematic analyses of water chemistry and the $\delta^{13}C_{DIC}$ were conducted to study the carbon biogeochemical process in the river-reservoir system. This study is useful to explore the carbon biogeochemical processes in karst river–reservoir systems and key factors affecting them, which will further support the building of global carbon cycle models under anthropogenic disturbance.

2. Materials and methods

2.1. Site description

The Pearl River is the 2nd largest river in China and 13th largest river in the world in terms of discharge, located at southern China at a latitude of 21.31–26.49°N and longitude of 102.14–115.53°E, with a drainage area of about 453,690 km^2. The annual flow can reach 330 $km^3\ year^{-1}$ which is about seven times higher than that of the Yellow River. The annual sunshine hours were 1282–2243 h and the average temperature and sunshine hours increased from upstream to downstream of the Pearl River. Moreover, the Pearl River basin is affected by the subtropical monsoon climate, with average annual temperature and precipitation of 14–22 °C and 1200–2200 mm, respectively. And more than 80% of the annual runoff occurs in the wet season (April to September) and < 20% occurs in the dry season (October to March). As altitude decreased, the average annual discharge of CST (48.4 $m^3\ s^{-1}$), LT (1639.4 $m^3\ s^{-1}$), YT (1760 $m^3\ s^{-1}$), and DH (1990 $m^3\ s^{-1}$) show a significant increase (Table 1). In the Pearl River basin minerals outcrop from Precambrian metamorphic rocks to Quaternary fluvial sediments. Permian and Triassic carbonate rock (e.g., limestone and dolomite) is widely distributed in the river basin and support the karst topography (Pu et al., 2020; Zhong et al., 2018). In this regard, we selected four reservoirs, viz. Chaishitan (CST), Longtan (LT), Yantan (YT), and Dahua (DH) with different regulation modes for the corresponding analysis. Out of four reservoirs under study (Table 1), CST is the first reservoir in the upper reaches of the Pearl River basin and LT is the second-largest reservoir in China. The short distance between LT, YT, and DH reservoirs can help to explore the cascading influence between the reservoirs. The reservoirs under study are mainly used for power generation and water transportation. Also, the Yunnan and Guangxi Province in the upstream area of the Pearl River belong to karst landforms (Fig. 1). The adequate precipitation and widely distributed canyon landforms in the karst river basins provide a firm structure for building dams. By the year 2018, large-scale reservoirs (number: 93) with a capacity over $10^8\ m^3$ and medium-sized reservoirs (number: 682) with a capacity from 10^7 to $10^8\ m^3$ have been built in the Pearl River basin with total water storage of 6.2 billion cubic meters (PRCMW, 2020).

2.2. Sampling and analysis

The water samples were collected at 15 locations (including two from tributaries) during April, July, and October of 2019 and January of 2020 to represent the spring, summer, autumn, and winter, respectively. The collected samples in each season from the mainstream (P1–P13) and its tributaries (T1, T2), of which P1, P4, P8, and P11 are the inlets, P2, P5, P6, P9, and P12 are the reservoir sites, P3, P7, P10, and P13 are the outlets of the reservoir (Fig. 1). The inflow and released water were collected at 0.5 m below the surface layer of the river and water profile samples were collected at different depths such as 0.5, 5, 15, 25, 30, 60, 90, and 135 m until reaching the bottom layer using a Niskin Water Sampler (Model 1010, General Oceanics, USA). Further, water pH, water temperature (T), dissolved oxygen (DO), and

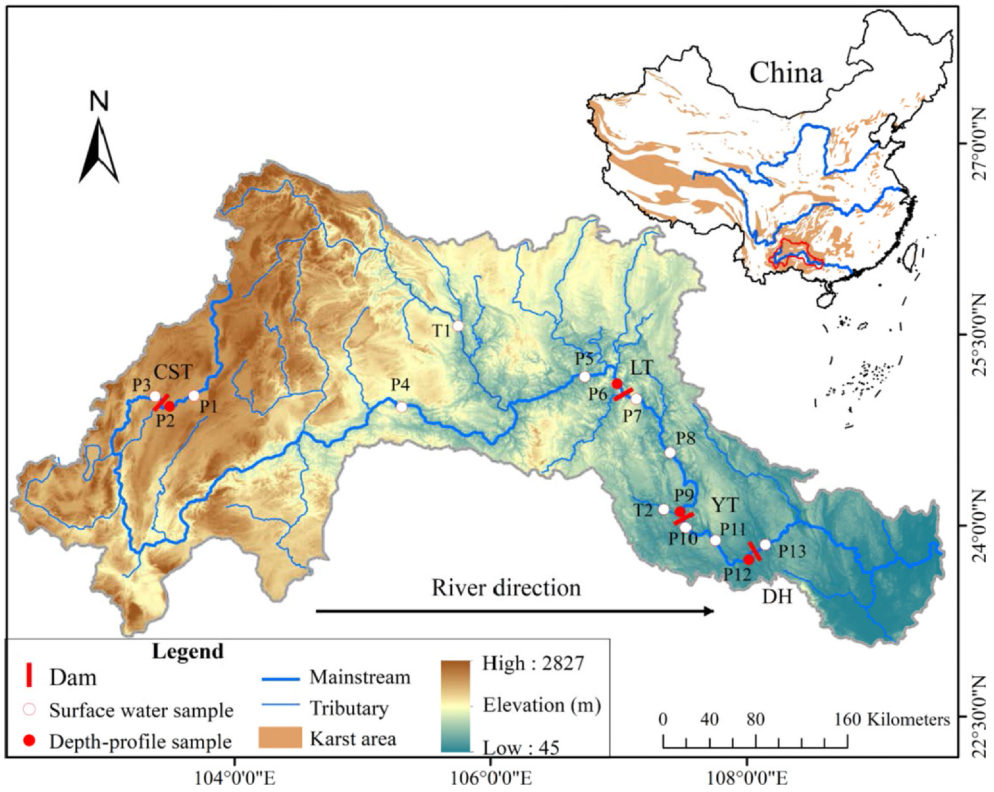

Fig. 1. Study area and sampling points in the Pearl cascade reservoirs of CST (Chaishitan reservoir), LT (Longtan reservoir), YT (Yantan reservoir), and DH (Dahua reservoir). Among the sampling sites, the capital letters "P" and "T" indicate sites located at Pearl River mainstream and its tributaries.

chlorophyll (Chl) were determined in situ by an automated multi-parameter profiler (model YSI EXO1). Water samples, except dissolved organic carbon (DOC), were filtered through a 0.45 μm membrane (Whatman, Inc.), whereas water samples for DOC analysis were filtered through 0.7 μm filter membrane (Waterman, GF/F), which was pre-heated at 450 °C. The filtered samples were packed in HDPE bottles and stored at −20 °C before analysis.

The total carbonate alkalinity was titrated with 0.02 mol L^{-1} hydrochloric acid within 12 h using a titrimeter (Brand 4760161) (Telmer and Veizer, 1999; Wang et al., 2020). The cation samples for Ca^{2+} analysis were acidified with purified HNO_3 to keep pH < 2 and then the samples were tested by the Inductively Coupled Plasma-Optical Emission Spectrometry (ICP-OES), with ± 5% uncertainty. The concentrations of DOC was analyzed using the Aurora 1030 TOC analyzer (OI Analytical, ± 5% uncertainty) with two replicates. The $\delta^{13}C_{DIC}$ sample was filtered in the field through 0.45 μm PTFE syringe filters and then injected 2 mL into a 12 mL vacuumed Labco bottle (containing 1 mL of 85% phosphoric acid) with three replicates to reduce the uncertainty. Further, $\delta^{13}C_{DIC}$ was tested by GasBench II device interfaced with an isotopic ratio mass spectrometer (IRMS, Finnigan Delta V) in the laboratory. The results were calibrated by the standards NBS-18 and expressed as a ‰ deviation from the standard Vienna Pee Dee Belemnite (V-PDB). The overall experimental accuracy for $\delta^{13}C$ measurements was ± 0.3‰. All samples were analyzed in the School of Earth System Science, Tianjin University. Flows and meteorological data were obtained online from the Ministry of Water Resources (www.mwr.gov.cn) and the China Meteorological Administration (www.cma.gov.cn).

2.3. Calculations methods

According to Henry's law, pCO_2 was expressed in μatm and calculated according to the following equation (Raymond et al., 1997; Telmer and Veizer, 1999):

$$pCO_2 = [H_2CO_3*]/K_{CO2} \quad (1)$$

where $[H_2CO_3*]$ means total concentrations of hydrated CO_2, and K_{CO2} is the Henry constant of CO_2 at a given temperature.

To reveal the main influencing factors and processes related to DIC migration and transformation in cascade reservoirs, the changing degree of DIC and Ca^{2+} was calculated according to the following equations (Wang et al., 2019b):

$$\Delta[DIC] = 100 \times ([DIC]_{sample} - [DIC]_{15m})/[DIC]_{15m}\,(\%) \quad (2)$$

$$\Delta[Ca^{2+}] = 100 \times ([Ca^{2+}]_{sample} - [Ca^{2+}]_{15m})/[Ca^{2+}]_{15m}\,(\%) \quad (3)$$

where $\Delta[DIC]$, $\Delta[Ca^{2+}]$ represent the changes of DIC and Ca^{2+} in depth-profiles compared with values at 15 m in the same water column.

The reservoir effect refers to the interaction between the reservoir and its hydrological factors, whose changes may relate to water depth, T, HRT, age, and other factors of the reservoirs (Li et al., 2018; Liang et al., 2019; St. Louis et al., 2000). Among the above parameters, water T and depth are used widely to indicate the reservoir effect and have attracted much attention from researchers (Boehrer and Schultze, 2008; Dubnyak and Timchenko, 2000). Previous studies determined the three different layers (epilimnion, thermocline, and hypolimnion) based on the variation of water T and have shown that the ratio of euphotic depth to mixing depth (Z_{eu}/Z_{mix}) can better indicate the strength of the thermal stratification (Liu et al., 2012; Kirk and Press, 1994). Besides, water depth is an important index affecting heat transfer and nutrient circulation (Dubnyak and Timchenko, 2000). Therefore, according to previous studies (Boehrer and Schultze, 2008; Wang et al., 2020; Liang et al., 2019; Liu et al., 2012), the reservoir effect index (R*i*, m^{-1}) was calculated based on the following equation in this study:

$$Ri = \Delta T \times 100/D = (T_S - T_B) \times 100/(T_S \times D) \quad (4)$$

where Ts is the surface temperature (°C), T_B represents bottom temperatures (°C), and D is the depth (m) of the reservoir.

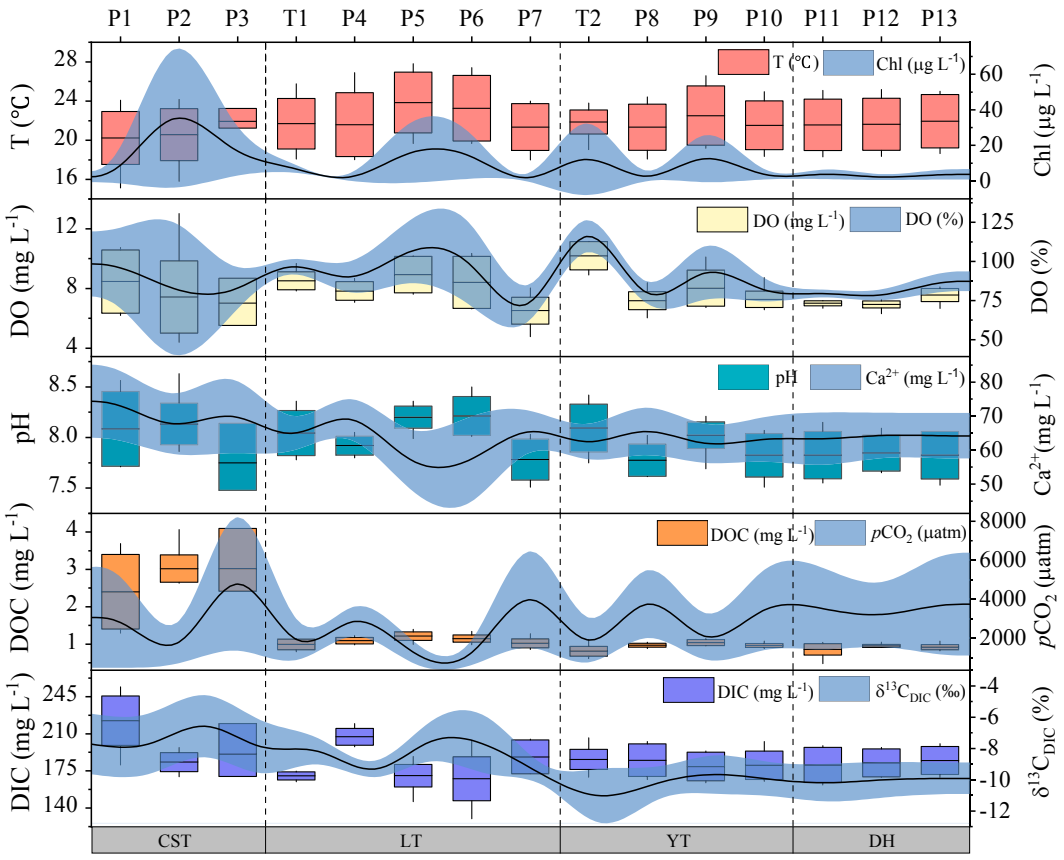

Fig. 2. Variations of water chemical parameters in surface water along the four cascade reservoirs in Pearl River. Analyzed data are presented as mean ± standard deviation. Boxes and whiskers plots for T (°C), DO (mg L^{-1}), pH, DOC (mg L^{-1}), and DIC (mg L^{-1}) at 25th to 75th and 10th to 90th percentiles, respectively. The central lines indicate that the median and outliers are not included. The x coordinate represents sampling points from P1 to P13 and tributaries of T1 and T2.

3. Results

3.1. Hydrological and physical characteristics

In the study year, the average inflow of CST (31.5 m^3 s^{-1}), LT (1777.8 m^3 s^{-1}), YT (1464.6 m^3 s^{-1}), and DH (1796.8 m^3 s^{-1}) reservoir were calculated and shown in Table 1. The HRT of CST, LT, YT, and DH were 103 days, 193 days, 21 days, and 5 days, respectively. The annual average air temperature ranged from 11 °C to 29.5 °C (mean = 22.4 °C, SD = 5.1 °C) during the sampling period. As a response, the surface water temperature ranged from 15.1 °C to 27.8 °C (mean = 21.8 °C, SD = 3.0 °C, Fig. 2). In the studied reservoirs of CST, LT, and YT, the average water temperature increased significantly from the fluvial area to the reservoir area, while the average water temperature remained stable in the DH reservoir (mean = 21.7 °C, SD = 2.9 °C). The outflow water temperature decreased significantly in the reservoirs of LT and YT but increased in the CST reservoir.

3.2. Spatiotemporal variations of water chemical parameters

The hydrochemical parameters of the cascade reservoirs from the CST (upstream) to the DH (downstream) reservoir showed significant spatiotemporal heterogeneities (Fig. 2). The DO concentrations ranged from 4.4 to 13.0 mg L^{-1} (mean = 7.6 mg L^{-1}, SD = 1.6 mg L^{-1}). Except for the DH reservoir, other reservoirs had a significant increase in the reservoir area and a decrease in the released water. However, the DO concentrations remained stable in the water column and ranged from 6.1 to 7.2 mg L^{-1} (mean = 6.8 mg L^{-1}, SD = 0.4 mg L^{-1}) in the DH reservoir (Figs. 2 and 3). The trend of reservoir surface water chemical parameters such as Chl (mean = 9.2 μg L^{-1}, SD = 15.3 μg L^{-1}), DO (%) (mean = 86.9%, SD = 18.5%), pH (mean = 7.9, SD = 0.3), and DOC (mean = 1.4 mg L^{-1}, SD = 0.9 mg L^{-1}) were similar to that of DO. However, the variations of Ca^{2+} (mean = 64.7 mg L^{-1}, SD = 8.4 mg L^{-1}) and pCO_2 (mean = 2937.1 μatm, SD = 1913.8 μatm) showed a reverse trend, whereas released water of the reservoirs with non-daily regulation increased significantly.

In the studied reservoirs, water chemical parameters varied in the lentic profiles (Fig. 3). In the wet season, the CST, LT and YT reservoirs showed significant thermal stratification in the lentic area and water T (mean = 19.3 °C, SD = 3.9 °C), DO (mean = 6.0 mg L^{-1}, SD = 3.2 mg L^{-1}), pH (mean = 7.8, SD = 0.3), Chl (mean = 10.0 μg L^{-1}, SD = 16.9 μg L^{-1}) and DOC (mean = 1.6 mg L^{-1}, SD = 0.9 mg L^{-1}) decreased significantly in the thermocline and remained stable in the hypolimnion. However, the concentrations of Ca^{2+} and pCO_2 were lower in the epilimnion and increased in the hypolimnion. The lowest value of pCO_2 (446 μatm) was found at the air–water interface of the CST, which was equivalent to the atmospheric value (i.e., ~400 μatm), and the highest value in the hypolimnion was 7324 μatm. In the dry season, the thermal stratification effect of the reservoirs was weaker than it during the wet season. Further, variation in the other water quality parameters such as water T (mean = 20.6 °C, SD = 3.8 °C), DO (mean = 4.9 mg L^{-1}, SD = 2.1 mg L^{-1}), pH (mean = 7.8, SD = 0.2), Chl (mean = 3.6 μg L^{-1}, SD = 5.6 μg L^{-1}) and DOC (mean = 1.5 mg L^{-1}, SD = 0.8 mg L^{-1}) fell with in a narrow range. The thermal stratification of water was still evident in the CST and LT reservoirs, and the highest value of pCO_2 (9804 μatm) appeared at the bottom (130 m) of the LT reservoir. As a whole, the hydrochemistry of the DH reservoir was similar to the river system, and there was no obvious variation in

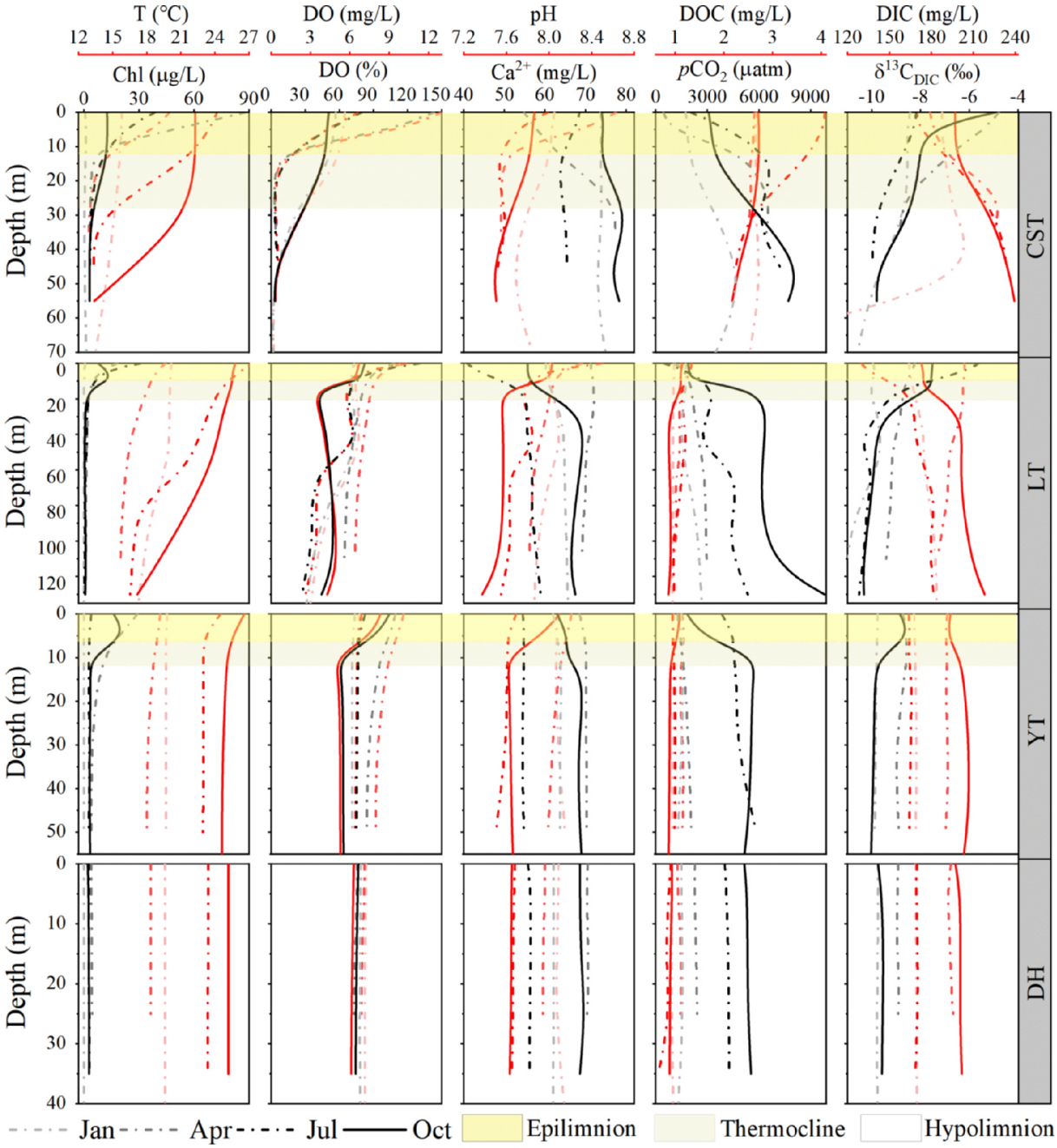

Fig. 3. The variations of water chemical data in the four stratified sampling profiles in different seasons.

the inflowing, stratified water, and the released water in the studied year.

3.3. DIC and $\delta^{13}C_{DIC}$

The DIC concentration (mean = 185.1 mg L^{-1}, SD = 21.5) in the lentic water surface area decreased significantly along the flow direction of cascade reservoirs (CST, LT, and YT), while it increased significantly in the released water. The highest value (129.8 mg L^{-1}) and the lowest value (254.2 mg L^{-1}) of DIC appeared in the CST and LT reservoirs, respectively. DIC concentrations tended to be stable in the YT (mean = 182.5 mg L^{-1}, SD = 16.0 mg L^{-1}) and the DH reservoir (mean = 183.8 mg L^{-1}, SD = 14.4 mg L^{-1}). The DIC concentration increased significantly along with the profiles of the CST, LT, and YT reservoirs and remained stable in the hypolimnion. In the wet season, the DIC concentration increased by 41.2% (129.8–183.2 mg L^{-1}) from epilimnion to hypolimnion in the LT reservoir and increased by 0.7% (194.0–195.4 mg L^{-1}) in the DH reservoir with shallow depth. However, DIC concentration in the hypolimnion of CST (254.2 mg L^{-1}) was much higher than that in the LT reservoir (183.2 mg L^{-1}). $\delta^{13}C_{DIC}$ (mean = −9.1‰, SD = 1.7‰) values decreased along the direction of water flow, which was contrary to that of DIC variation. The values of $\delta^{13}C_{DIC}$ were significantly higher in the lentic surface area (mean = −7.2‰, SD = 1.9‰) than the fluvial area (mean = −8.5‰, SD = 1.6‰) of the CST and the LT reservoirs, and it decreased significantly in the released water (mean = −9‰, SD = 1.5‰). Further, the highest value of $\delta^{13}C_{DIC}$ was −4.8‰ in the epilimnion of CST whereas the lowest value was −13.4‰ in the released water of the YT reservoir. The average $\delta^{13}C_{DIC}$ in the DH reservoir (mean = −10.0‰, SD = 1.0‰) was significantly lower than that in the other reservoirs (mean = −9.1‰, SD = 1.5‰) and with little variation.

Table 2
Relationships between DIC concentrations, $\delta^{13}C_{DIC}$, and related environmental parameters in the water column of studied reservoirs.

		Depth (m)			T (°C)			pH			DO (mg L^{-1})			DOC (mg L^{-1})			Chl (μg L^{-1})		
		R2	p	n	R2	p	n	R2	p	n	R2	p	n	R2	p	n	R2	p	n
CST	DIC	**0.764**	< 0.001	23	**0.371**	0.002	23	**0.393**	0.001	23	**0.533**	< 0.001	23	**0.397**	0.001	23	**0.276**	0.010	23
	δ^{13}CDIC	**0.561**	< 0.001	23	*0.211*	0.028	23	**0.404**	0.001	23	**0.531**	< 0.001	23	0.011	0.636	23	**0.456**	< 0.001	23
LT	DIC	*0.164*	0.019	33	**0.294**	0.001	33	0.175	0.016	33	0.037	0.285	33	**0.324**	< 0.001	33	*0.137*	0.034	33
	δ^{13}CDIC	**0.430**	< 0.001	33	**0.382**	< 0.001	33	**0.245**	0.003	33	**0.343**	< 0.001	33	**0.501**	< 0.001	33	**0.621**	< 0.001	33
YT	DIC	0.030	0.420	24	0.050	0.293	24	0.001	0.887	24	0.000	0.947	24	0.005	0.745	24	0.126	0.089	24
	δ^{13}CDIC	0.016	0.560	24	0.142	0.069	24	**0.564**	< 0.001	24	**0.345**	0.003	24	**0.374**	0.001	24	**0.353**	0.002	24
DH	DIC	0.005	0.779	19	0.028	0.496	19	0.068	0.283	19	**0.537**	< 0.001	19	*0.220*	0.043	19	**0.332**	0.010	19
	δ^{13}CDIC	0.003	0.816	19	*0.241*	0.033	19	*0.261*	0.025	19	0.028	0.496	19	**0.581**	< 0.001	19	0.036	0.436	19

Where n: number of samples; p: significance level; *correlation was significant at the 0.01 level (marked in bold)
**correlation was significant at the 0.05 level (marked in italics).

3.4. Reservoir effect index

The correlation analysis was performed in related environmental parameters with DIC concentrations and $\delta^{13}C_{DIC}$ in the studied cascade reservoirs, and the results showed that water depth and temperature were significantly correlated with DIC and $\delta^{13}C_{DIC}$ in the reservoirs of long HRT (CST and LT reservoirs) (Table 2). Moreover, there was no significant correlation in the reservoirs of short HRT (YT and DH reservoir). The reservoir effect index (R*i*) of the four reservoirs was estimated as 0.66 (CST), 0.21 (LT), 0.10 (YT), and 0 (DH). Besides, R*i* values depended on seasonal variability and were found to be larger in the wet season than in the dry season. The largest value ($Ri = 1.02$) was observed in April at the CST reservoir and the lowest ($Ri = 0$) was in the DH reservoir.

4. Discussion

4.1. Cascade damming effect on DIC concentrations and $\delta^{13}C_{DIC}$

DIC and $\delta^{13}C_{DIC}$ values showed obvious spatial heterogeneities along with the cascade reservoirs (Figs. 2 and 3). The ranges of DIC concentrations and $\delta^{13}C_{DIC}$ in the lentic area of reservoirs were much wider than those in the fluvial area (Fig. 2). These variations suggest that damming on karst river systems plays a significant role in carbon biogeochemical processes. The relative mechanisms and underlying processes are discussed below.

In natural karst rivers, DIC is mainly derived from weathering of carbonate rocks, which leads to the higher DIC concentration than non-karst rivers (Gaillardet et al., 2019; Liu and Han, 2020). The sampling point P1 is not affected by damming and the average DIC concentrations was higher than the reservoir surface samples in the study year, which is similar to the inflow water of the Hongjiadu reservoir in the Wujiang River (Wang et al., 2020). However, the construction of dams hindered the water velocity, resulting in increased water surface temperature with a long HRT (Wang et al., 2019b). The variations in concentrations of DIC and Ca^{2+} help in characterizing the migration and transformation of carbon in rivers (Binet et al., 2020; Wang et al., 2019b; Zhong et al., 2020). In this study, DIC and Ca^{2+} showed similar trends at different water depths, having a significant positive correlation ($R^2 = 0.64$, Fig. 4(a)). The DIC and Ca^{2+} concentrations in the epilimnion of LT and CST reservoirs were lower than those in the hypolimnion. It suggested that the calcium carbonate ($CaCO_3$) precipitation and dissolution are two important processes in the epilimnion and hypolimnion, respectively. However, DIC and Ca^{2+} concentrations were more concentrated, with seasonal differences in the YT and DH reservoirs, which suggest that reservoirs with short HRTs may have limited influence on water chemical parameters (Fig. 4(a)).

A pattern diagram has been presented to understand the biogeochemical processes that affect the behavior of carbon (Fig. 4). It was found that DIC, Ca^{2+}, and $\delta^{13}C_{DIC}$ could be used to explain the exact processes involved in the river–reservoir system (Wang et al., 2019b, 2020). In this study, the significant positive relationship of Δ[DIC] and $\Delta[Ca^{2+}]$ could help to understand the processes that affected the DIC transport and transformation in different reservoirs (Fig. 4(b)). Due to human regulation and air temperature increases, the water temperature increased significantly in the epilimnion after forming a stable thermal stratification in the reservoirs of CST, LT, and YT in the wet season. The results showed that $\delta^{13}C_{DIC}$ values became heavy in the epilimnion of the above three reservoirs, and the DIC and Ca^{2+} decreased simultaneously. Moreover, the surface high Chl contents and DO (%) > 100 in the wet season of the three reservoirs, indicating that the process of phytoplankton photosynthesizes in the epilimnion. The photosynthesis of phytoplankton can consume DIC (e.g., HCO_3^- and CO_2 (aq)) and prefer to use the lighter ^{12}C, resulting in heavy $\delta^{13}C_{DIC}$ and high pH (Maberly et al., 2012; Pu et al., 2020). The significant positive relationship between Chl and $\delta^{13}C_{DIC}$ further indicates that the carbon was influenced by the primary productivity in the DH, LT, and YT reservoirs (Table 2). Moreover, intense phytoplankton photosynthesis would increase the absorption of shortwave light, which could slow down the heat transfer in the profile (Dubnyak and Timchenko, 2000; Boehrer and Schultze, 2008). Therefore, the epilimnion is much shallower than other layers (Fig. 3), and the hydrochemical parameters (e.g., water T, PH and DO) varied notably (Wang et al., 2020; Cui et al., 2017). The saturated status of $CaCO_3$ was formed under high pH and water temperature conditions, which leads to a decrease of Ca^{2+} and DIC in the epilimnion (Liu et al., 2018; Wang et al., 2020). Further, the rapid decrease of DIC content and the increase of pH could cause low pCO_2, due to the phytoplankton photosynthesis in the epilimnion of CST, LT, and YT reservoirs (Jiang et al., 2020; Pu et al., 2020). However, all measured data was distributed around the origin of the DH reservoir with a short HRT, indicating a weak damming effect on water chemistry (Fig. 4(b)). The above results suggested that the epilimnion of the LT, CST, and YT reservoirs with obvious thermal stratification was mainly affected by phytoplankton photosynthesis, $CaCO_3$ precipitation, and CO_2 outgassing, which were mainly distributed in the first quadrant (Fig. 4(b)). In the second quadrant (Fig. 4(b)), Δ[DIC] increased while $\Delta[Ca^{2+}]$ and $\delta^{13}C_{DIC}$ decreased, indicating that DIC may be affected by both groundwater input and OM degradation (Vachon et al., 2020). In the third quadrant (Fig. 4(b)), pH, T, Chl and DO decreased significantly, while DIC and pCO_2 increased significantly, indicating that DIC in the water may be mainly from the degradation of OM and dissolution of $CaCO_3$ of samples from the thermocline and hypolimnion (Binet et al., 2020). Besides, $\delta^{13}C_{DIC}$ was found to be negative in the thermocline and hypolimnion, which further proved that OM degradation was one of the key processes affecting DIC concentration. Therefore, high pCO_2 in thermocline and hypolimnion would lead to CO_2 outgassing and provid CO_2 for phytoplankton photosynthesis in the epilimnion. As a response, primary production also produced DO and OM, which helped in the process of OM oxidizing and decomposing in the thermocline and hypolimnion. In the fourth

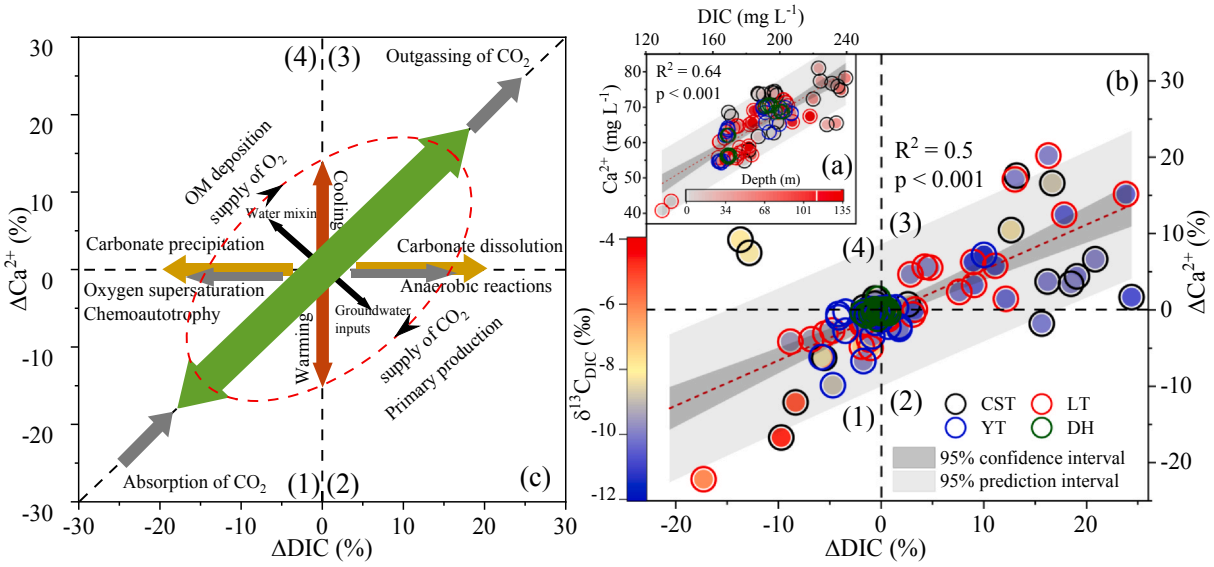

Fig. 4. (a) The relationship between DIC (mg L^{-1}) and Ca^{2+} (mg L^{-1}) for depth samples in the four reservoirs. (b) The relationship between Δ[DIC] and Δ[Ca^{2+}] for depth samples in the four reservoirs. (c) The pattern diagram by means of hydrochemistry and $\delta^{13}C_{DIC}$. The four quadrants (1, 2, 3, and 4) show the processes affecting DIC.

quadrant (Fig. 4(b)), decreased Δ[DIC] and increased Δ[Ca^{2+}] may be caused by rainfall and mixing of water in the process of water flowing from river to reservoir area, which was mainly reflected in the lentic surface of the CST reservoir (Wang et al., 2020; Zeng et al., 2020).

In the mainstream along the water flow direction of the cascade reservoirs, pH, DIC, and DOC decreased while pCO_2 increased, indicating that the regional damming effect with a long HRT and high air temperature may enhance the carbon emission in the downstream (Wang et al., 2020). Moreover, pH and DO decreased significantly whereas pCO_2 increased rapidly in the released water of the CST, LT, and YT reservoirs, indicating that the rapid influx of atmospheric O_2 with a high air temperature will accelerate the degradation of OM and cause a increase in pCO_2 (Pu et al., 2020). Due to the high air temperature in July, thermal stratification was most obvious in reservoirs with a long HRT and showed similar characteristics of cascade reservoirs built on the Wujiang River and Jialing River (Cui et al., 2017; Wang et al., 2020). Taking the site P1 ($\delta^{13}C_{DIC}$ = −10.6‰) with no damming effect as a reference, $\delta^{13}C_{DIC}$ decreased to −13.4‰ in the YT reservoir in July. However, $\delta^{13}C_{DIC}$ increased to −11.3‰ in the DH reservoir where the annual average was −9.9 ± 0.9‰. Our results showed a similar trend with other karst cascade reservoirs in the Wujiang river (−8.8‰ to −10.1‰) and the Jialing river (−12.3‰ to −12.7‰) (Cui et al., 2017; Wang et al., 2020). The above results showed that dam construction may cause a regional damming effect (the increase of pCO_2 and decrease both pH and $\delta^{13}C_{DIC}$) and further help to understand its effect on the carbon cycle. However, when thermal stratification became weak in the downstream, the water chemical characteristics would be similar to the natural river system. In this case, the impact of the reservoirs on carbon biogeochemical processes may depend on the reservoir itself, and the regional damming effect was localized in the river-reservoir system.

4.2. The enlightenment of reservoir effect index on carbon biogeochemical processes

Previous studies revealed that the effect of river damming on nutrients was influenced by HRT, reservoir age, latitude, climate, and water depth (Grill et al., 2019; Maavara et al., 2020; St. Louis et al., 2000; Kumar et al., 2019) but no clear standard for the impact assessment of river damming has been reported yet. $\delta^{13}C_{DIC}$ is widely used in studying carbon evolution in inland waters as an indicator to understand the geochemical behavior of carbon (Maberly et al., 2012; Pu et al., 2020; Telmer and Veizer, 1999; Zhang and Liu, 2014). In this study, hydrochemistry and isotope indicate that DIC was mainly affected by the weathering of carbonate rocks in the fluvial area, due to high DIC content and light $\delta^{13}C_{DIC}$ values (Li et al., 2008; Liu and Han, 2020; Zhong et al., 2018). In the reservoirs with obvious thermal stratification, DIC was mainly influenced by primary productivity and OM degradation in the epilimnion and hypolimnion (Maberly et al., 2012; Wang et al., 2020). Moreover, most of the water is discharged from the bottom of dams, which is mainly from the hypolimnion. Therefore, DIC is mainly affected by CO_2 outgassing, OM degradation, and carbonate dissolution (Kumar et al., 2019; Mendonça et al., 2017; Wang et al., 2019b). In this study, we found that both water depth and water temperature had positive relationships with DIC and $\delta^{13}C_{DIC}$ in the CST and the LT reservoir, displaying a thermal stratification effect (Table 2). Water temperature is one of the most important drivers for the formation of thermal stratification in river–reservoir systems (Elçi, 2008; Liang et al., 2019). In this study, the water depth of the LT reservoir was up to 135 m, which is much deeper than that of fluvial area (< 10 m), resulting in variability of water temperature at different depths. Besides, the elevation difference between the CST and DH reservoirs is 1485 m, causing the annual average air temperature difference of 6.4 °C and then leading to difference in water column temperature (Table 1). It further suggested that the reservoir effect cannot be characterized directly by the different reservoirs' water temperatures.

From the above discussion, the damming effect on water thermal stratification may be better characterized by the R*i* (ratio of ΔT to Depth) as shown in Eq. (4). And it is found that R*i* has a strong linear relationship with $\delta^{13}C_{DIC}$, which are found to be high in the reservoirs with a long HRT (Fig. 5(a)). However, R*i* and $\delta^{13}C_{DIC}$ values are not found to be high in the LT reservoir with the longest HRT, which suggests that although HRT is an important driver, it may not be the determining factor. Since the 1990s, CO_2 emissions from reservoirs have attracted much attention, and OC degradation was regarded as an important source of CO_2 (Duchemin et al., 1995; Kumar et al., 2019; Li et al., 2018; Raymond et al., 2013; St. Louis et al., 2000). Moreover, the DOC concentration is much higher than that of the Chishui River, which is not influenced by the damming effect in the karst area (Xu et al., 2020). In this study, R*i* and DOC had a good linear relationship, and with the increase of R*i*, DOC concentration increased and pCO_2

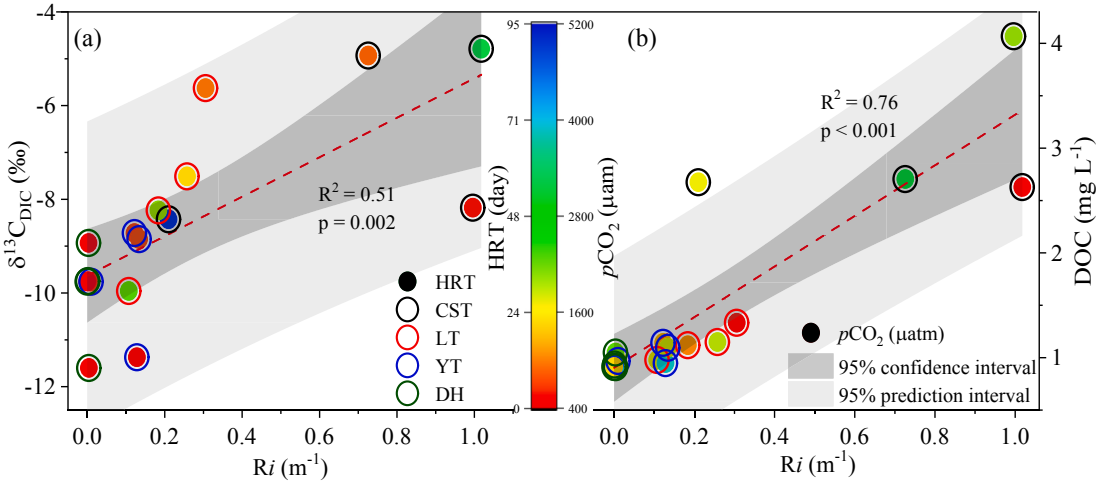

Fig. 5. (a) $\delta^{13}C_{DIC}$ versus Reservoir effect index (R*i*), and (b) DOC (mg L^{-1}) versus R*i* in surface water of the four cascade reservoirs.

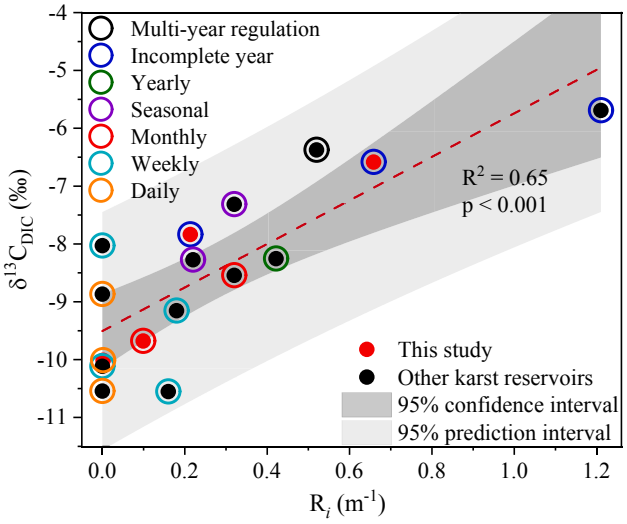

Fig. 6. $\delta^{13}C_{DIC}$ versus Reservoir effect index (R*i*). The data consist of mean of each reservoir and is symbolized by solid color circles. The hollow-colored circles represent reservoirs with different hydraulic retention time (HRT).

decreased, indicating that R*i* can be an important index to investigate the strength of primary productivity which would further help to understand the processes behind the carbon cycle (Fig. 5(b)). To test the indicative role of R*i* in other karst reservoirs, we compiled data of cascade reservoirs in the mainstream of the Wujiang River, Jialing River, and the HF reservoir of the Maotiao river, and plotted them together with the data in this study (Cui et al., 2017; Wang et al., 2016, 2020). The results show that R*i* and $\delta^{13}C_{DIC}$ have a positive relationship (R^2 = 0.65, p < 0.001) (Fig. 6), which reveal that $\delta^{13}C_{DIC}$ in the surface water is distinctly different in the reservoirs with different HRTs. Further, it indicates that $\delta^{13}C_{DIC}$ of reservoirs with similar HRT also have significant differences, which suggest that reservoir effect also depends on the reservoir characteristics.

Generally, large R*i* represents a strong reservoir effect, which is mainly reflected in the significant thermal stratification of the reservoir. The R*i* can also help to explain why the highest value of pCO_2 occurred in the reservoir hypolimnion of LT reservoir in October. In October, the stratification of the water may be more pronounced due to the longer HRT, higher temperature, and less disturbance by precipitation in the LT reservoir. The R*i* value in January (0.14), April (0.20), July (0.40), and October (0.33) further indicate that the LT reservoir still had a strong reservoir effect in October (Fig. 4). Moreover, intensified phytoplankton photosynthesis in the epilimnion and accelerated degradation of OM in the hypolimnion, resulted in higher pCO_2 in the released water, which suggest that R*i* can better explore the reservoir effect by combining the hydrochemical characteristics and geographical characteristics. Therefore, compared with HRT, the application of both R*i* and isotopic signatures will help to investigate the strength of the damming effect on the carbon cycle and further provide theoretical support for the evaluation of the reservoir effect in karst areas.

5. Conclusion

In this study, four cascade reservoirs in the subtropical region were selected to study the effect of damming on riverine carbon transport and the underlying processes using water chemistry and stable isotopic signatures of dissolved inorganic carbon ($\delta^{13}C_{DIC}$). Results revealed that after cascade damming in karst rivers, the main influence processes of DIC in karst rivers were transformed from carbonate weathering to the jointly regulation by carbonate weathering, carbonate precipitation, primary production, and OM degradation. After a comprehensive analysis of hydrochemistry and $\delta^{13}C_{DIC}$, we proposed the concept of reservoir effect index (R*i*), which is a more sensitive indicator than HRT and could provide a more accurate indication of damming effect on the carbon cycle and inherent processes involved. By compiling $\delta^{13}C_{DIC}$ of other karst reservoirs, it is proved that R*i* can be used to represent the stratification strength of reservoirs and further help to understand the degree of damming effect on the carbon cycle. Our study can act as a reference for other karst damming rivers to assess the impact of damming on the carbon cycle so that mitigation measures could be implemented in advance to reduce its emission in the future. However, numerous factors affect the carbon characteristics after building dams on rivers, therefore, additional work needs to be done in the future such as multi-isotope analyses, higher frequency monitoring, and application of hydrodynamics, which will help to further understand the migration and transformation of carbon in river-reservoir systems.

CRediT authorship contribution statement

Wanfa Wang: Formal analysis, Methodology, Writing - original draft. **Yuanbi Yi:** Investigation, Writing - original draft. **Jun Zhong:** Conceptualization, Project administration, Writing - review & editing. **Amit Kumar:** Writing - review & editing. **Si-Liang Li:** Supervision, Funding acquisition, Writing - review & editing.

Declaration of Competing Interest

The authors declare that they have no known competing financial interests or personal relationships that could have appeared to influence the work reported in this paper.

Acknowledgments

This work was supported by the National Key R&D Program of China (Grant No. 2016YFA0601002), National Natural Science Foundation of China (Grant No. 41925002), Tianjin Research Innovation Project for Postgraduate Students (Grant No. 2019YJSB183), and Strategic Priority Research Program of Chinese Academy of Sciences (Grant No. XDB40020200). We are thankful to Shiyuan Ding, Zenglei Han, and Pengbin Chen for their help during the field work. And we thank Sen Xu, Sainan Chen, and Shuai Chen for editing the English text.

References

Barros, N., Cole, J.J., Tranvik, L.J., Prairie, Y.T., Bastviken, D., Huszar, V.L., et al., 2011. Carbon emission from hydroelectric reservoirs linked to reservoir age and latitude. Nat. Geosci. 4, 593. https://doi.org/10.1038/ngeo1211.

Best, J., 2018. Anthropogenic stresses on the world's big rivers. Nat. Geosci. 12, 7–21. https://doi.org/10.1038/s41561-018-0262-x.

Beaulieu, E., Goddéris, Y., Donnadieu, Y., Labat, D., Roelandt, C., 2012. High sensitivity of the continental-weathering carbon dioxide sink to future climate change. Nat. Clim. Change. 2, 346–349. https://doi.org/10.1038/nclimate1419.

Binet, S., Probst, J.L., Batiot, C., Seidel, J.L., Emblanch, C., Peyraube, N., et al., 2020. Global warming and acid atmospheric deposition impacts on carbonate dissolution and CO_2 fluxes in French karst hydrosystems: evidence from hydrochemical monitoring in recent decades. Geochim. Cosmochim. Acta 270, 184–200. https://doi.org/10.1016/j.gca.2019.11.021.

Boehrer, B., Schultze, M., 2008. Stratification of lakes. Rev. Geophys. 46. https://doi.org/10.1029/2006rg000210.

Cardinale, B.J., Duffy, J.E., Gonzalez, A., Hooper, D.U., Perrings, C., Venail, P., et al., 2012. Biodiversity loss and its impact on humanity. Nature 486, 59–67. https://doi.org/10.1038/nature11148.

Cole, J.J., Prairie, Y.T., Caraco, N.F., McDowell, W.H., Tranvik, L.J., Striegl, R.G., et al., 2007. Plumbing the global carbon cycle: integrating inland waters into the terrestrial carbon budget. Ecosystems 10, 171–184. https://doi.org/10.1007/s10021-006-9013-8.

Cui, G.Y., Li, X.D., Li, Q.K., Huang, J., Tao, Y.L., Li, S.Q., et al., 2017. Damming effects on dissolved inorganic carbon in different kinds of reservoirs in Jialing River, Southwest China. Acta Geochim. 36, 581–597. https://doi.org/10.1007/s11631-017-0155-5.

Dams, W.C.O., 2000. Dams and Development: A NEW Framework for Decision-making: The Report of the World Commission on Dams. Earthscan, 2000.

Duchemin, E., Lucotte, M., Canuel, R., Chamberland, A., 1995. Production of the greenhouse gases CH_4 and CO_2 by hydroelectric reservoirs of the boreal region. Global Biogeochem. Cy. 9, 529–540. https://doi.org/10.1029/95GB02202.

Dubnyak, S., Timchenko, V., 2000. Ecological role of hydrodynamic processes in the Dnieper reservoirs. Ecol. Eng. 16, 181–188. https://doi.org/10.1016/S0925-8574(00)00103-8.

Elçi, Ş., 2008. Effects of thermal stratification and mixing on reservoir water quality. Limnology 9, 135–142. https://doi.org/10.1007/s10201-008-0240-x.

Fan, H., He, D.M., Wang, H.L., 2015. Environmental consequences of damming the mainstream Lancang-Mekong River: a review. Earth-Sci. Rev. 146, 77–91. https://doi.org/10.1016/j.earscirev.2015.03.007.

Ford, D., Williams, P., 2007. In: Karst Hydrogeology and Geomorphology. Wiley, London. https://doi.org/10.1002/9781118684986.

Gaillardet, J., Calmels, D., Romero-Mujalli, G., Zakharova, E., Hartmann, J., 2019. Global climate control on carbonate weathering intensity. Chem. Geol. 527. https://doi.org/10.1016/j.chemgeo.2018.05.009.

Grill, G., Lehner, B., Thieme, M., Geenen, B., Tickner, D., Antonelli, F., et al., 2019. Mapping the world's free-flowing rivers. Nature 569, 215–221. https://doi.org/10.1038/s41586-019-1111-9.

ICOLD, 2018. Number of Dams by Country Members. International Commission on Large Dams. (World Register of Dams).

Jiang, Y.J., Lei, J.Q., Hu, L.C., Xiao, Q., Wang, J.L., Zhang, C., et al., 2020. Biogeochemical and physical controls on the evolution of dissolved inorganic carbon (DIC) and $\delta^{13}C_{DIC}$ in karst spring-waters exposed to atmospheric CO_2(g): insights from laboratory experiments. J. Hydrol. 583. https://doi.org/10.1016/j.jhydrol.2019.124294.

Jiang, Z.C., Lian, Y.Q., Qin, X.Q., 2014. Rocky desertification in Southwest China: impacts, causes, and restoration. Earth-Sci. Rev. 132, 1–12. https://doi.org/10.1016/j.earscirev.2014.01.005.

John, I.H., 1992. Global biogeochemical cycles: progress and problems. Mar. Chem. https://doi.org/10.1016/0304-4203(92)90096-S.

Kirk, J.T.O., Press, C., 1994. Light and photosynthesis in aquatic ecosystems. J. Ecol. 45, 349–350. https://doi.org/10.2307/2261578.

Kondolf, G.M., Rubin, Z.K., Minear, J.T., 2014. Dams on the Mekong: cumulative sediment starvation. Water Resour. Res. 50, 5158–5169. https://doi.org/10.1002/2013wr014651.

Kumar, A., Yang, T., Sharma, M.P., 2019. Long-term prediction of greenhouse gas risk to the Chinese hydropower reservoirs. Sci. Total Environ. 646, 300–308. https://doi.org/10.1016/j.scitotenv.2018.07.314.

Li, S.Y., Bush, R.T., Santos, I.R., Zhang, Q.F., Song, K.S., Mao, R., et al., 2018. Large greenhouse gases emissions from China's lakes and reservoirs. Water Res. 147, 13–24. https://doi.org/10.1016/j.watres.2018.09.053.

Li, S.L., Calmels, D., Han, G.L., Gaillardet, J., Liu, C.Q., 2008. Sulfuric acid as an agent of carbonate weathering constrained by $\delta^{13}C_{DIC}$: Examples from Southwest China. Earth Planet. Sci. Lett. 270, 189–199. https://doi.org/10.1016/j.epsl.2008.02.039.

Liang, X., Xing, T., Li, J.X., Wang, B.L., Wang, F.S., He, C.Q., et al., 2019. Control of the hydraulic load on nitrous oxide emissions from cascade reservoirs. Environ. Sci. Technol. 53, 11745–11754. https://doi.org/10.1021/acs.est.9b03438.

Liu, J.K., Han, G.L., 2020. Effects of chemical weathering and CO_2 outgassing on $\delta^{13}C_{DIC}$ signals in a Karst watershed. J. Hydrol. https://doi.org/10.1016/j.jhydrol.2020.125192.

Liu, M.X., Xu, X.L., Wang, D.B., Sun, A.Y., Wang, K., 2016. Karst catchments exhibited higher degradation stress from climate change than the non-karst catchments in southwest China: an ecohydrological perspective. J. Hydrol. 535, 173–180. https://doi.org/10.1016/j.jhydrol.2016.01.033.

Liu, Z.H., Macpherson, G.L., Groves, C., Martin, J.B., Yuan, D.X., Zeng, S.B., 2018. Large and active CO_2 uptake by coupled carbonate weathering. Earth-Sci. Rev. 182, 42–49. https://doi.org/10.1016/j.earscirev.2018.05.007.

Liu, L., Liu, D.F., Xiao, S.B., Kong, S., Chen, Y.Y., Fang, X.F., 2012. Effects of thermal stratification on spring blooms in Xiangxi bay of the Three Gorges Reservoir. Environ. Sci. 3046–3050 (in Chinese).

Maavara, T., Chen, Q.W., Van Meter, K., Brown, L.E., Zhang, J.Y., Ni, J.R., et al., 2020. River dam impacts on biogeochemical cycling. Rev. Earth & Environ Nat. https://doi.org/10.1038/s43017-019-0019-0.

Maavara, T., Lauerwald, R., Regnier, P., Van Cappellen, P., 2017. Global perturbation of organic carbon cycling by river damming. Nat. Commun. 8, 15347. https://doi.org/10.1038/ncomms15347.

Maberly, S.C., Barker, P.A., Stott, A.W., De Ville, M.M., 2012. Catchment productivity controls CO_2 emissions from lakes. Nat. Clim. Change 3, 391–394. https://doi.org/10.1038/nclimate1748.

Mendonça, R., Müller, R.A., Clow, D., Verpoorter, C., Raymond, P., Tranvik, L.J., et al., 2017. Organic carbon burial in global lakes and reservoirs. Nat. Commun. 8. https://doi.org/10.1038/s41467-017-01789-6.

Meybeck, M., 1982. Carbon, nitrogen, and phosphorus transport by world rivers. Am. J. Sci. 282, 401–450. https://doi.org/10.2475/ajs.282.4.401.

Olden, J.D., Naiman, R.J., 2010. Incorporating thermal regimes into environmental flows assessments: modifying dam operations to restore freshwater ecosystem integrity. Freshw. Biol. 55, 86–107. https://doi.org/10.1111/j.1365-2427.2009.02179.x.

PRCMW, 2020. Water resources bulletin 2018. < http://www.pearlwater.gov.cn/ > . (accessed date: 20 February 2020) (in Chinese).

Pu, J.B., Li, J.H., Zhang, T., Martin, J.B., Yuan, D.X., 2020. Varying thermal structure controls the dynamics of CO_2 emissions from a subtropical reservoir, south China. Water Res. 178, 115831. https://doi.org/10.1016/j.watres.2020.115831.

Raymond, P.A., Caraco, N.F., Cole, J.J., 1997. Carbon dioxide concentration and atmospheric flux in the Hudson River. Estuaries 20, 381–390. https://doi.org/10.2307/1352351.

Raymond, P.A., Hartmann, J., Lauerwald, R., Sobek, S., McDonald, C., Hoover, M., et al., 2013. Global carbon dioxide emissions from inland waters. Nature 503, 355–359. https://doi.org/10.1038/nature12760.

REN21. Renewables 2016. Global Status Report. REN21. < https://www.ren21.net/gsr-2016/ > .

St. Louis, V.L., Kelly, C.A., Duchemin, É., Rudd, J.W.M., Rosenberg, D.M., 2000. Reservoir surfaces as sources of greenhouse gases to the atmosphere: a global estimate. Bioscience 50. https://doi.org/10.1641/0006-3568(2000)050.

Telmer, K., Veizer, J., 1999. Carbon fluxes, pCO_2 and substrate weathering in a large northern river basin, Canada: carbon isotope perspectives. Chem. Geol. 159, 61–86. https://doi.org/10.1016/S0009-2541(99)00034-0.

Tockner, K., Stanford, J.A., 2002. Riverine flood plains: present state and future trends. Environ. Conserv. 29, 308–330. https://doi.org/10.1017/s037689290200022x.

Vachon, D., Sadro, S., Bogard, M.J., Lapierre, J.F., Baulch, H.M., Rusak, J.A., et al., 2020. Paired O_2–CO_2 measurements provide emergent insights into aquatic ecosystem function. Oceanogr. Lett Limnol. https://doi.org/10.1002/lol2.10135.

Wang, B.L., Zhang, H.T., Liang, X., Li, X.D., Wang, F.S., 2019a. Cumulative effects of cascade dams on river water cycle: evidence from hydrogen and oxygen isotopes. J. Hydrol. 568, 604–610. https://doi.org/10.1016/j.jhydrol.2018.11.016.

Wang, F.S., Maberly, S.C., Wang, B.L., Liang, X., 2018. Effects of dams on riverine biogeochemical cycling and ecology. Inland Waters 8, 130–140. https://doi.org/10.1080/20442041.2018.1469335.

Wang, S.L., Yeager, K.M., Lu, W.Q., 2016. Carbon isotope fractionation in phytoplankton as a potential proxy for pH rather than for [CO_2(aq)]: Observations from a carbonate lake. Limnol. Oceanogr. 61, 1259–1270. https://doi.org/10.1002/lno.10289.

Wang, W.F., Li, S.L., Zhong, J., Li, C., Yi, Y.B., Chen, S.N., et al., 2019b. Understanding transport and transformation of dissolved inorganic carbon (DIC) in the reservoir system using $\delta^{13}C_{DIC}$ and water chemistry. J. Hydrol. 574, 193–201. https://doi.org/10.1016/j.jhydrol.2019.04.036.

Wang, W.F., Li, S.L., Zhong, J., Maberly, S.C., Li, C., Wang, F.S., et al., 2020. Climatic and anthropogenic regulation of carbon transport and transformation in a karst river-reservoir system. Sci. Total Environ. 707, 135628. https://doi.org/10.1016/j.

scitotenv.2019.135628.
Xu, S., Li, S.L., Zhong, J., Li, C., 2020. Spatial scale effects of the variable relationships between landscape pattern and water quality: example from an agricultural karst river basin, Southwestern China. Agric. Ecosyst. Environ. 300. https://doi.org/10.1016/j.agee.2020.106999.
Yoshikawa, S., Cho, J., Yamada, H.G., Hanasaki, N., Kanae, S., 2014. An assessment of global net irrigation water requirements from various water supply sources to sustain irrigation: rivers and reservoirs (1960–2050). Hydrol. Earth Syst. Sci. 18, 4289–4310. https://doi.org/10.5194/hess-18-4289-2014.
Zeng, J., Han, G.L., Wu, Q.X., Tang, Y., 2020. Effects of agricultural alkaline substances on reducing the rainwater acidification: Insight from chemical compositions and calcium isotopes in a karst forests area. Agric. Ecosyst. Environ. 290. https://doi.org/10.1016/j.agee.2019.106782.
Zhang, D., Liu, C.Q., 2014. A preliminary study on sulfate reduction bacteria behaviors in groundwater by sulfur and carbon isotopes: a case study in Jiaozuo City, China. Ecotoxicology 23, 2014–2024. https://doi.org/10.1007/s10646-014-1330-7.
Zhong, J., Li, S.L., Liu, J., Ding, H., Sun, X.L., Xu, S., et al., 2018. Climate variability controls on CO_2 consumption fluxes and carbon dynamics for monsoonal rivers: evidence from Xijiang River, Southwest China. J. Geophys. Res. Biogeosci. 123, 2553–2567. https://doi.org/10.1029/2018jg004439.
Zhong, J., Li, S.L., Ibarra, D.E., Ding, H., Liu, C.Q., 2020. Solute production and transport processes in Chinese monsoonal rivers: Implications for global climate change. Global Biogeochem. Cy. 34. https://doi.org/10.1029/2020gb006541.